Atmospheric Research 171 (2016) 31–40

Contents lists available at ScienceDirect

Atmospheric Research

journal homepage: www.elsevier.com/locate/atmosres

A new method of satellite-based haze aerosol monitoring over the North China Plain and a comparison with MODIS Collection 6 aerosol products

Xing Yan [a,b], Wenzhong Shi [a,*], Nana Luo [c], Wenji Zhao [b]

[a] Department of Land Surveying and Geo-Informatics, The Hong Kong Polytechnic University, Hong Kong
[b] College of Resource Environment and Tourism, Capital Normal University, Beijing, China
[c] Department of Geography, San Diego State University, USA

ARTICLE INFO

Article history:
Received 15 September 2015
Received in revised form 2 December 2015
Accepted 4 December 2015
Available online 14 December 2015

Keywords:
Haze
Aerosol optical thickness
Retrieval algorithm
Modis

ABSTRACT

With worldwide urbanization, hazy weather has been increasingly frequent, especially in the North China Plain. However, haze aerosol monitoring remains a challenge. In this paper, MODerate resolution Imaging Spectroradiometer (MODIS) measurements were used to develop an enhanced haze aerosol retrieval algorithm (EHARA). This method can work not only on hazy days but also on normal weather days. Based on 12-year (2002–2014) Aerosol Robotic Network (AERONET) aerosol property data, empirical single scattering albedo (SSA) and asymmetry factor (AF) values were chosen to assist haze aerosol retrieval. For validation, EHARA aerosol optical thickness (AOT) values, along with MODIS Collection 6 (C6) dark-pixel and deep blue aerosol products, were compared with AERONET data. The results show that the EHARA can achieve greater AOT spatial coverage under hazy conditions with a high accuracy (73% within error range) and work a higher resolution (1-km). Additionally, this paper presents a comprehensive discussion of the differences between and limitations of the EHARA and the MODIS C6 DT land algorithms.

1. Introduction

Haze is defined as a weather phenomenon in which air has a relative humidity of ≤80% and atmospheric visibility of <10 km (World Meteorological Organization, WMO). Thick haze is detrimental to the environment and public health (Hoek et al., 2010). In recent years, due to rapid worldwide urbanization, haze has become a serious problem in many countries. In China in particular, increased industrialization and fossil-fuel consumption have caused serious particulate-matter (PM) pollution, resulting in frequent haze. The increase in haze has been associated with mortality and morbidity from respiratory diseases and cardiovascular problems (Ram et al., 2014). Haze can contain high concentrations of heavy metals and PM, which are thought to be the most harmful pollution components (Huang et al., 2012). Thus, mitigation of haze pollution has become a crucial challenge for environmental management agencies in urban areas. In this context, the sources and spatial distribution of haze are of particular concern.

Many studies have been performed to analyze the physical and chemical characteristics of haze (Che et al., 2009; Huang et al., 2011; Sun et al., 2006). However, most studies have been based on ground and point measurements, which lack spatial coverage and may not elucidate the sources contributing to the formation of haze in widespread areas (Tao et al., 2012). To overcome this limitation, satellite remote sensing can be used to monitor and describe the spatial variability of regional haze. In recent studies, the Moderate Resolution Imaging Spectroradiometer (MODIS) has been widely applied in the field of haze analysis due to its large spatial and temporal coverage (Lee et al., 2006a; Lee et al., 2006b; Noh et al., 2009; Tao et al., 2014). For example, Tao et al. (2012) provided large-scale and long-term insights into regional haze over the North China Plain of Eastern China using MODIS data, and Han et al. (2013) proposed an enhanced dust index for Asian dust detection.

Using satellite imagery to monitor haze aerosol optical thickness is also an effective way to assess air pollution levels. The MODIS atmosphere Level 2 aerosol product has been widely used and shown a high accuracy. It has three aerosol retrieval algorithms: dark-target (DT) land algorithm, DT ocean algorithm and deep-blue (DB) algorithm. However, the aerosol model on hazy days is very different from that on less-polluted days, the default aerosol model in the DT land algorithm of MODIS Aerosol Optical Thickness (AOT) products may be not suitable. In addition, hazy weather conditions are always accompanied by a thick aerosol layer, which causes uncertainty in the relationship between the visible (VIS) and the short-wave infrared (SWIR) bands, but it is still used in the DT land algorithm of the MODIS AOT products. Lee et al. (2006b) also found that using the MODIS SWIR-to-VIS ratio to determine surface reflectance over Northeast Asia could lead to errors in aerosol retrieval. In order to monitor haze distribution, Li et al. (2013) presented an AOT retrieval method for heavy haze events based on a

* Corresponding author at: ZS628, The Department of Land Surveying and GeoInformatics, The Hong Kong Polytechnic University, Hung Hom, Kowloon, Hong Kong.
E-mail address: lswzshi@polyu.edu.hk (W. Shi).

http://dx.doi.org/10.1016/j.atmosres.2015.12.003
0169-8095/

lookup table (LUT) method; however, the maximum retrieval of AOT by this method is 3.0, while in Beijing the AOT will be more than 5.0 on some hazy days, such as on July 6, 2014. Thus, accurate AOT retrieval is still a difficult task under hazy weather conditions. In addition, although many current aerosol retrievals make use of the LUT, it is time consuming when building it (Li et al., 2005; Wong et al., 2011; Zha et al., 2011). Tang et al. (2005) used the synergy of Terra and Aqua MODIS data (SYNTEM) to obtain AOTs in China without an LUT, but the results tended to be poor when there was an obvious difference in weather conditions between two observation passes. Luo et al. (2015) proposed an improved aerosol retrieval algorithm with fast calculation and reliable outcomes; however, the method is based on Landsat images and intended for urban-scale studies, and is not suitable for haze aerosol monitoring of larger areas.

The purpose of this study is to develop a new algorithm to obtain aerosol conditions; it includes haze identification, retrieval of AOT not only on hazy days but also in normal weather. A comprehensive discussion of the differences and limitations of this method compared with the C6 DT land algorithm is also presented in this study.

2. Data and methods

2.1. Study area

The North China Plain is the largest alluvial plain in China, with an area of 409,500 km^2, as shown in Fig. 1. The region includes Beijing, Tianjin, and Hebei, whose gross domestic product accounted for 11.3% of China's GDP in 2007. With the development of urbanized construction, the land cover in the North China Plain has changed markedly. Many main roads and residential buildings have been built to accommodate the increase in motor vehicles and in population. Even though the government has made great efforts to improve the environment, urban air pollution problems have become increasingly serious. Particulate matter levels are severe around the cities and continuous air-pollution episodes such as haze events are more frequent than in the past (Li et al., 2013).

2.2. Satellite data

Daytime MODIS TERRA satellite images were acquired (https://ladsweb.nascom.nasa.gov/data/search.html) from December 2013 to June 2015, as shown in Table 1. TERRA is a satellite launched in 1999 that passes from north to south over the study area every morning (ca. 10:30 a.m. local time); with 36 wavebands, it can be used for atmospheric, oceanic, and land studies at both global and local scales.

Collection 6 MODIS aerosol products (C6 MOD04) were obtained for this study, and C6 DT AOT with 10-km and 3-km resolution (Optical_Depth_Land_And_Ocean) were used as a comparison. In addition, MODIS C6 DB AOT with 10-km resolution (Deep_Blue_Aerosol_Optical_Depth_550_land_Best_Estimate) was also obtained for comparison, which was filtered by quality assurance (QA) (Hsu et al., 2013; Sayer et al., 2013). The C6 cloud mask data (Aerosol_Cldmsk_Land_Ocean) were extracted from MOD04 and used for cloud detection in our algorithm.

The MODIS Albedo product (MCD43) was also acquired. It provides data describing both directional hemispherical reflectance (black-sky albedo) and bi-hemispherical reflectance (white-sky albedo). The MCD43A1 Bi-directional Reflection Distribution Function (BRDF)/Albedo Model Parameters Product provides the weighting parameters associated with the Ross Thick–LiSparse Reciprocal BRDF model. These three parameters (fiso, fvol, and fgeo) are provided for each of the MODIS spectral bands. In this study, fiso, fvol, and fgeo in Bands 1 and 3 were collected to calculate surface reflectance.

2.3. Enhanced haze aerosol retrieval algorithm (EHARA)

A new method is described here for haze monitoring and AOT retrieval based on MODIS data. This algorithm is designed for application in large areas characterized by the complex land surfaces of cities or

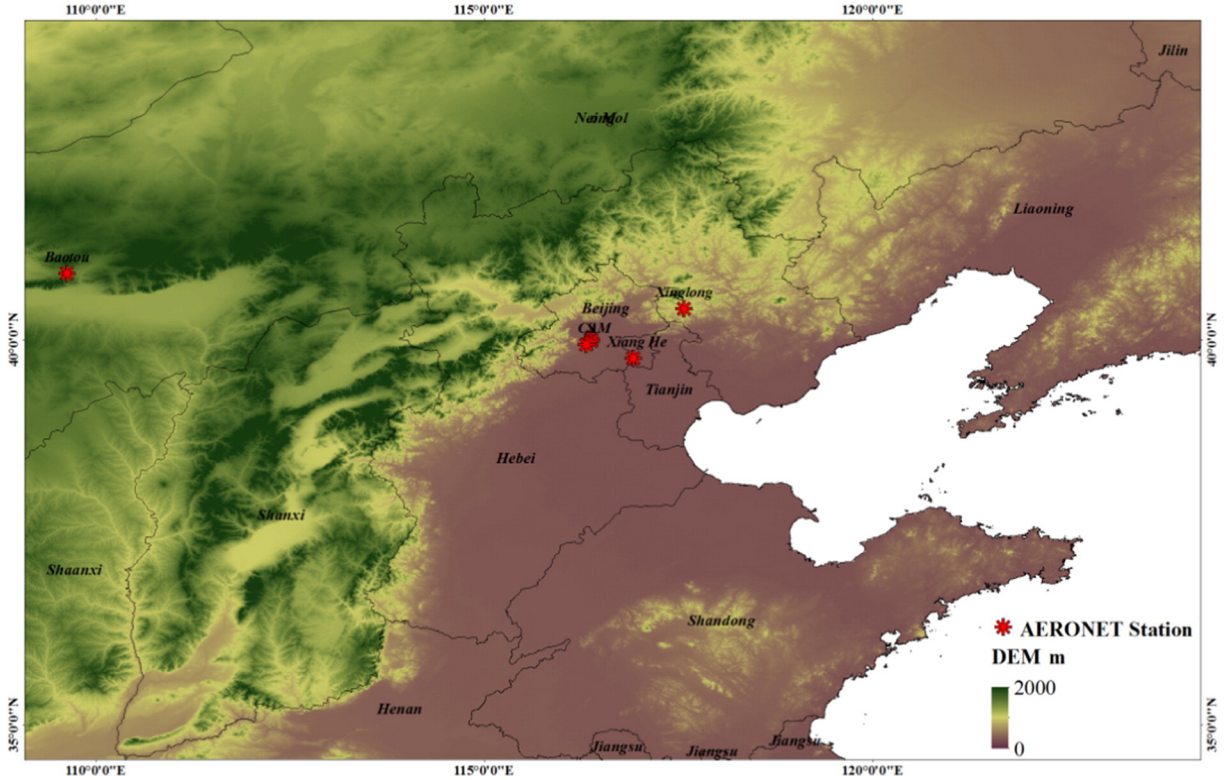

Fig. 1. Study area.

Table 1
The MODIS data used in this study.

MODIS	Date	Month	Year	AERONET Station[a]	Date	Month	Year	AERONET Station[a]
TERRA	11	12	2013	BJ, BR,BC	16	10	2014	BR,XH
	12	12	2013	BJ, BR	17	10	2014	BC,BR
	14	12	2013	BJ,BR	18	10	2014	BJ,BC,BR,XH
	26	12	2013	BJ,BR	25	10	2014	BC,BR,BT,XH
	28	12	2013	BJ,BR	13	11	2014	BJ,BC,BR
	30	12	2013	BJ,BR,BC	17	11	2014	BJ,BR,BC
	1	1	2014	BJ,BR	22	11	2014	BJ,BR,BC
	3	1	2014	BJ,BR,BC	26	11	2014	BJ,BC,BR,XH
	13	1	2014	BJ,BR,BC	1	12	2014	BR,BC
	22	1	2014	BJ,BR,BC	3	12	2014	BR,BC
	3	2	2014	BJ,XH	17	12	2014	BJ,BR
	4	2	2014	BJ,BR	24	12	2014	BJ,BR,BC
	27	2	2014	BR,XH	31	12	2014	BJ,BR,BC
	2	3	2014	BR,XH	2	1	2015	BJ,BR,BC
	14	3	2014	BJ,BR	6	1	2015	BJ,BC
	22	3	2014	BJ,XH	11	1	2015	BJ,BR,BC
	7	4	2014	BJ,XH	27	1	2015	BJ,BC
	2	5	2014	BJ,BC,XH	30	1	2015	BJ,BR,BC
	7	5	2014	BJ,BC,XH	5	2	2015	BJ,BR,BC
	16	5	2014	BJ,XH	17	2	2015	BJ,BR,BC
	18	5	2014	BJ,XH	26	2	2015	BJ,BR,BC
	3	6	2014	BJ,BC	3	3	2015	BJ,BR,BC
	12	6	2014	BJ,BC	11	3	2015	BR,BC
	27	6	2014	BJ,BC	21	3	2015	BJ,BC
	28	6	2014	BJ,XH	23	3	2015	BC,XH
	5	7	2014	BJ,BC,XH	21	4	2015	BC,XH
	6	7	2014	BJ,BC,XH	22	4	2015	BC,XH
	10	7	2014	BJ,BC	24	4	2015	BJ,BR,BC
	12	7	2014	BJ,BC	26	4	2015	BR,BC
	15	8	2014	BJ,BC	4	5	2015	BJ,BR,BC
	25	8	2014	BC,XH	7	5	2015	BJ,BR,BC
	3	9	2014	BR,BC	19	5	2015	BJ,BR,BC
	8	9	2014	BJ,BR,BC	26	5	2015	BJ,BR,BC
	9	9	2014	BJ,BR	2	6	2015	BR,BC
	15	9	2014	BJ,BR	8	6	2015	BJ,BC
	9	10	2014	BC,BR,BT,XH	18	6	2015	BJ,BR,BC
	10	10	2014	BC,BR,BT,XH				

[a] BJ = Beijing AERONET station; BR = Beijing-RADI AERONET station; BC = Beijing-CAMS AERONET station; XL = Xinglong AERONET station; XH = Xiang He AERONET station; BT = AOE_Baotou AERONET station.

dense vegetation. A schematic diagram of this method is shown in Fig. 2. The central idea of this algorithm is dependent on the spectral characteristics received by a satellite to detect haze, and it then uses an aerosol model to calculate AOT. In this method, haze detection rules of MODIS image is based on Table 1 in Li et al. (2013).

Initially MODIS L1B data have a gas-absorption correction, as does the latest C6 method, based on Appendix A in Levy et al. (2013). The EHARA is described as follows. The MODIS-measured TOA spectral reflectance can be estimated by (Drury et al., 2008):

$$\rho_{TOA(\lambda)}(\theta_0,\theta,\phi)=\rho_{Aer}(\theta_0,\theta,\phi)+\rho_{Ray}(\theta_0,\theta,\phi)+\frac{T_{(\theta_0)}T_{(\theta)}\rho_s(\theta_0,\theta,\phi)}{1-\rho_s(\theta_0,\theta,\phi)S_{(\lambda)}} \quad (1)$$

where θ_0 is the solar zenith, θ is the sensor view zenith, and ϕ is the relative azimuth angle, $\rho_{Aer}(\theta_0,\theta,\phi)$ is the aerosol reflectance, $\rho_{Ray}(\theta_0,\theta,\phi)$ is the Rayleigh reflectance for molecules, $T_{(\theta_0)}$ and $T_{(\theta)}$ are the downward and upward total scattering transmittances, and $S_{(\lambda)}$ is the atmospheric backscattering ratio. $T_{(\theta_0)}$ and $T_{(\theta)}$ are defined by:

$$\left.\begin{aligned}T_{(\theta_0)}&=\exp\left[\frac{-(\tau_R+\tau_a)}{\mu_s}\right]+t_d(\mu_s)\\T_{(\theta)}&=\exp\left[\frac{-(\tau_R+\tau_a)}{\mu_v}\right]+t_d(\mu_v)\end{aligned}\right\} \quad (2)$$

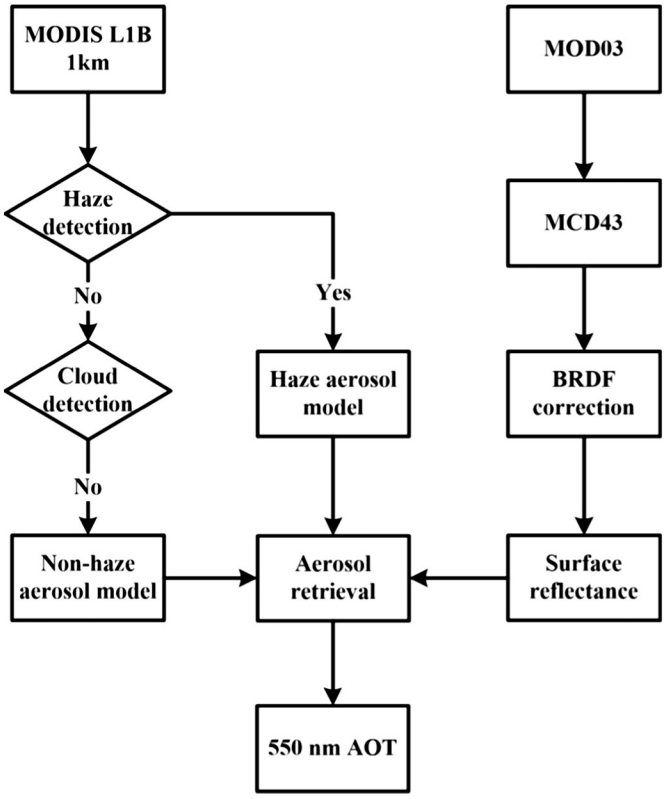

Fig. 2. Schematic diagram for the EHARA.

where μ_s is the cosine of the solar zenith angle, μ_v is the cosine of the sensor zenith angle and τ_a is the AOT. τ_R is the Rayleigh optical depth, which can be calculated as follows:

$$\tau_R=0.00864\lambda^{-\left(3.916+0.074\lambda+\frac{0.05}{\lambda}\right)} \quad (3)$$

$t_d(\mu)$ is the diffuse transmittance and can be well approximated by (Liu and Liu, 2009; Tanre et al., 1979):

$$t_d(\mu)=\exp(-(\tau_R+\tau_a)/\mu)\{\exp[(0.52\tau_R+\tau_a(1+g)/2)/\mu]-1\} \quad (4)$$

For the atmospheric backscattering ratio $S_{(\lambda)}$, it can be approximated by:

$$S_\lambda=(0.92\tau_R+(1-g)\tau_a)\exp[-(\tau_R+\tau_a)] \quad (5)$$

in which g is the asymmetry factor (AF).

$\rho_{Aer}(\theta_0,\theta,\phi)$ is the aerosol reflectance in the absence of air molecules, which results from single scattering; it can be approximated by (Antoine and Morel, 1998):

$$\rho_{Aer}(\theta_0,\theta,\phi)=\frac{\omega_0\tau_a P_a(\theta_0,\theta,\phi)}{4\mu_s\mu_v} \quad (6)$$

where ω_0 is the single scattering albedo (SSA), $P_a(\theta_0,\theta,\phi)$is the aerosol scattering phase function as (Rahman et al., 1993):

$$P_a(\theta_0,\theta,\phi)=\frac{1-g^2}{[1+g^2-2g\cos(\pi-\Theta)]^{\frac{3}{2}}} \quad (7)$$

Then, the Rayleigh reflectance for molecules $\rho_{Ray}(\theta_0,\theta,\phi)$ can be approximated by (Antoine and Morel, 1998):

$$\rho_{Ray}(\theta_0,\theta,\phi)=\frac{\omega_R\tau_R P_R(\theta_0,\theta,\phi)}{4\mu_s\mu_v} \tag{8}$$

where ω_R is the Rayleigh single-scattering albedo; in this study, $\omega_R\approx 1$. $P_R(\theta_0,\theta,\phi)$ is the Rayleigh scattering phase function as (Levy et al., 2007):

$$P_R(\theta_0,\theta,\phi)=\frac{3}{4}(1+\cos^2(\Theta)) \tag{9}$$

with

$$\Theta=\cos^{-1}(-\cos(\theta_0)\cos(\theta)+\sin(\theta_0)\sin(\theta)\cos(\phi)). \tag{10}$$

Thus, AOT (τ_a) can be calculated by:

$$\tau_a=\frac{4\mu_s\mu_v\left\{\rho_{TOA(\lambda)}-\frac{\omega_R\tau_R P_R}{4\mu_s\mu_v}-\frac{T_{(\theta)}T_{(\theta_0)}\rho_s}{1-\rho_s[0.92\tau_R+(1-g)\tau_a]exp[-(\tau_R+\tau_a)]}\right\}}{\omega_0 P_a} \tag{11}$$

In Eq. (11), the surface reflectance (ρ_s) is a key parameter in the aerosol retrieval algorithm. In this study, surface reflectance was calculated by MCD43 at corresponding MODIS L1b data angles (Roujean et al., 1992). In EHARA, we used the single-scatter approximation for aerosol reflectance as Eqs. (6) and (7), and a BRDF assumption for surface reflectance. Then EHARA combined these with a multiple-scattered light equation over a Lambertian surface as Eq. (1). However, it should be noted that the physical assumptions in EHARA are not as self-consistent as DB and DT with a full radiative transfer model.

2.4. 2.6 Aerosol model

The aerosol model varies significantly in different areas and seasons. The SSA and the asymmetry factor (AF) are two key parameters in determining aerosol physical properties. The SSA and AF may differ for each pixel in MODIS data due to large coverage (Drury et al., 2008). Thus, in this study, we determined the SSA and AF values for each pixel from the nearest AERONET station (Table 1). If the nearest AERONET station's measurements were under hazy conditions, the non-hazy areas used empirical SSA and AF values based on last years' mean value in the corresponding season. On the other hand, if the nearest AERONET station's measurements were under non-hazy conditions, the hazy areas were assigned empirical SSA and AF values, as will be discussed in detail in Section 3.1.

3. Results

3.1. Haze aerosol model

To obtain empirical SSA and AF values for haze aerosol retrieval, 12-yr. (2002–2014) AERONET data for hazy days in Beijing were collected. Fig. 3 shows SSA values at 440 nm and 675 nm under hazy conditions. It is evident that 675-nm SSA values are always higher than 440-nm SSA values, which means that aerosol particles are more strongly scattered at 675 nm on hazy days. From 2002 to 2006, SSA was low in these two wavelengths. Lee et al. (2006a) also found that the haze aerosol had a large absorption (SSA = 0.88) with black carbon particles in October 2004. After 2007, the SSA values at 675 nm (total mean SSA at 675 nm) were generally above 0.90, with the highest mean value of 0.95 in 2012, which approximates to the dust model in the MODIS retrieval algorithm (Levy et al., 2010). The mean SSA value at 440 nm in these years was always between 0.89 and 0.91, which was a little higher than the total mean value of 0.89. The SSA values increase when the haze aerosol displays more scattering and the secondary aerosols include both sulfate and nitrate (Yan et al., 2008). Thus, the empirical SSA for the haze aerosol model in this study were 0.9 (blue band) and 0.92 (red band), values that are consistent with the results of previous studies (Noh et al., 2009; Tao et al., 2013; Tao et al., 2014). It is interesting that SSA has been higher over Beijing area in recent years. Yu et al. (2012) found that from 2002 to 2008, the mean values of haze SSA were 0.91 (675 nm) and 0.89 (440 nm). And in the normal days, Bergin et al. (2001) indicated that SSA over Beijing in 1999 was 0.81 and Mao and Li (2005) showed that the mean SSA was 0.79 in 2003. Fig. 4 shows the AF variation at 440 nm and 675 nm, clearly showing that AF values were higher at 440 nm than at 675 nm, and always ranged from 0.69 to 0.71, which approximates to the total mean value of 0.7. AF mean values were always between 0.65 and 0.66, similar to the 12-yr mean value of 0.66. Therefore, the empirical AF in this study was 0.71 for the blue band and 0.67 for the red band (Tanre et al., 1979).

3.2. Haze aerosol optical thickness retrieval

To illustrate the outcomes of the EHARA, we use three retrieval results as examples. The first case is under heavy haze conditions. Fig. 5A is a true-color satellite image taken on 9 October 2014, which shows significantly different colors that distinguish heavy haze and cloud. Generally, clouds are white and haze appears gray. The haze mark based on Li et al. (2013) is shown in Fig. 5B, with extensive

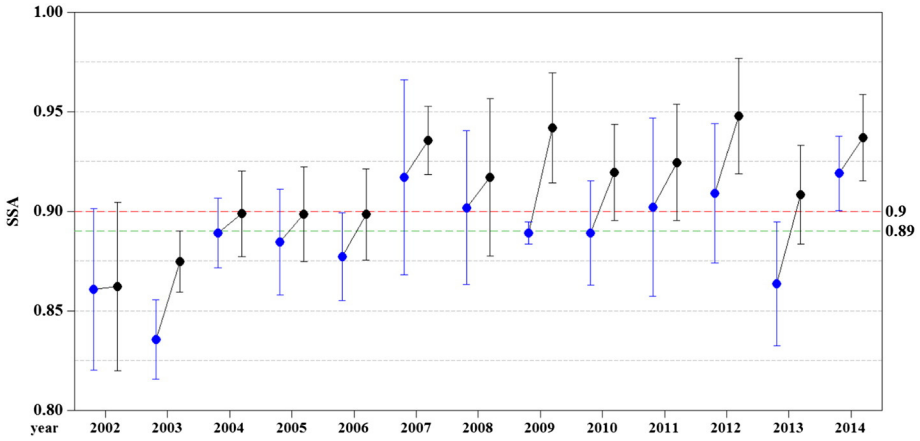

Fig. 3. Interval plot of haze SSA from 2002 to 2014 (95% confidence interval; the black points are SSA at 675 nm wavelength; the blue points are SSA at 440 nm wavelength; the red dashed line is the mean SSA at 675 nm over the 12 years, and the green dashed line is the mean SSA value at 440 nm over the 12 years). (For interpretation of the references to color in this figure legend, the reader is referred to the web version of this article.)

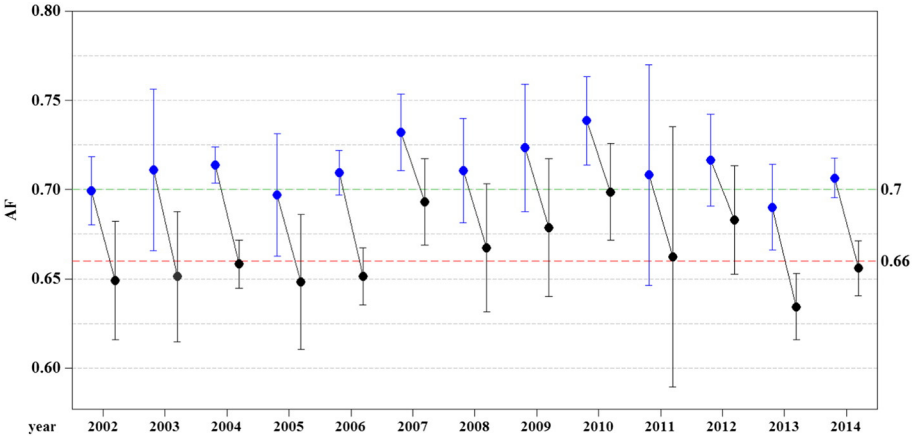

Fig. 4. Interval plot of haze AF values from 2002 to 2014 (95% confidence interval; the black points are AF at 675 nm wavelength; the blue points are AF at 440 nm wavelength; the red dashed line is the mean AF value at 675 nm over the 12 years, and the green dashed line is the mean AF value at 440 nm over the 12 years). (For interpretation of the references to color in this figure legend, the reader is referred to the web version of this article.)

coverage over Beijing, Hebei, and Shanxi. Fig. 5F presents the EHARA 1-km AOT spatial distribution for the same day, revealing a high haze aerosol-loading event over the North China Plain. High AOT values (2.5–3) are evident between Beijing and Hebei due to the local topography, which forms a bowl ringed by mountainous terrain (Yanshan and Taihang mountains) in the west (Lee et al., 2006a). When the atmospheric structure is stable, air masses are easily blocked by these mountains, which leads to haze accumulation.

The second case is a hazy day with cloud. Fig. 6A shows cloudy weather conditions over the North China Plain on 5 July 2014. Haze detection revealed scattered haze pixels that covered a wide, area including Beijing, Tianjin, Hebei, Shanxi, Henan, and Shandong (Fig. 6B). Fig. 6F shows the high aerosol values (AOT: 4–5.5) over the Beijing, Liaoning, Hebei, and Shandong regions, where values were much higher than in the northwestern areas (AOT: 0.2–0.4).

The third case is under normal weather conditions on 16 October 2014. The true-color satellite image shows a fine and cloud-free day on the North China Plain (Fig. 7A). No haze pixels were detected, indicating good weather conditions (Fig. 7B). Fig. 7F shows that high AOT values were observed in southeastern areas with high population

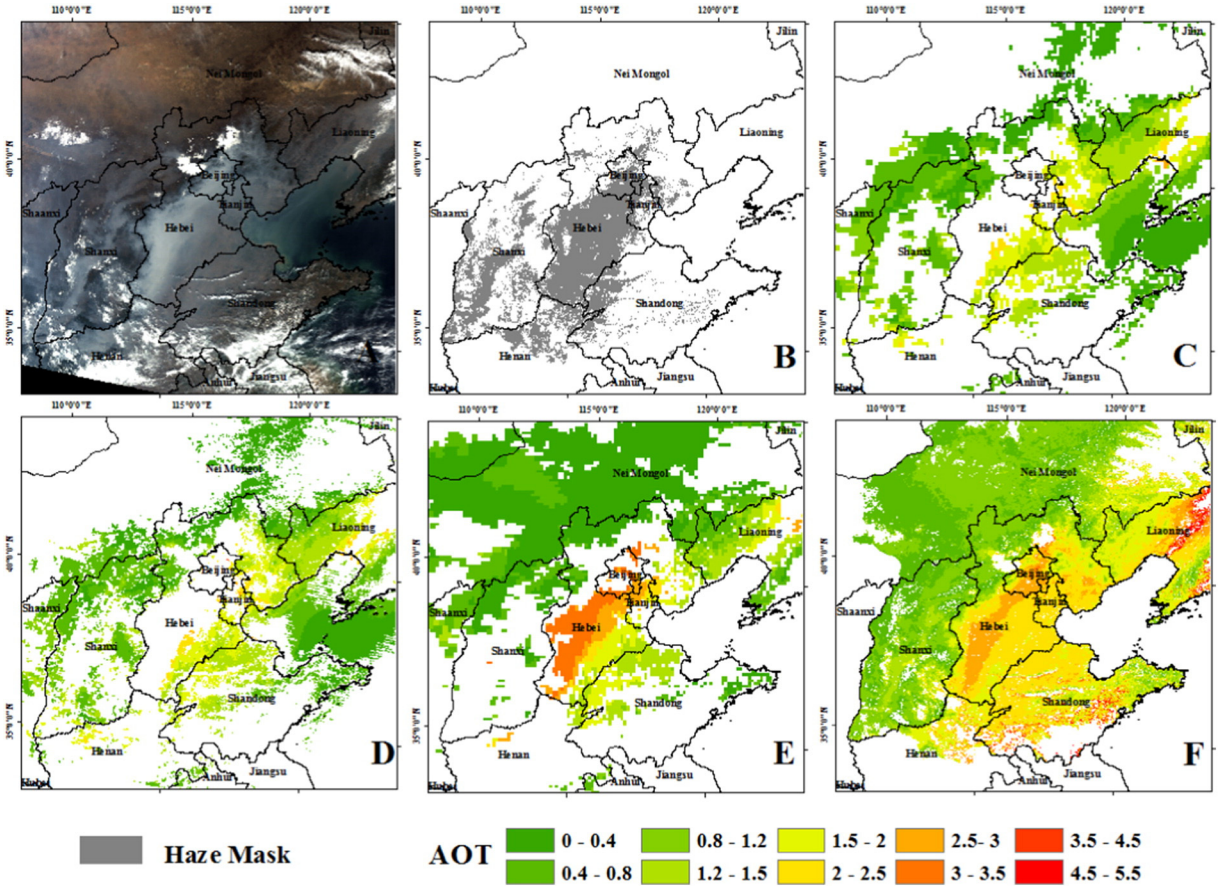

Fig. 5. (A) True-color MODIS image taken on 9 October 2014. (B) Result of haze identification. (C) MODIS C6 DT 10-km AOT. (D) MODIS C6 3-km AOT. (E) MODIS C6 DB 10-km AOT. (F) EHARA 1-km AOT.

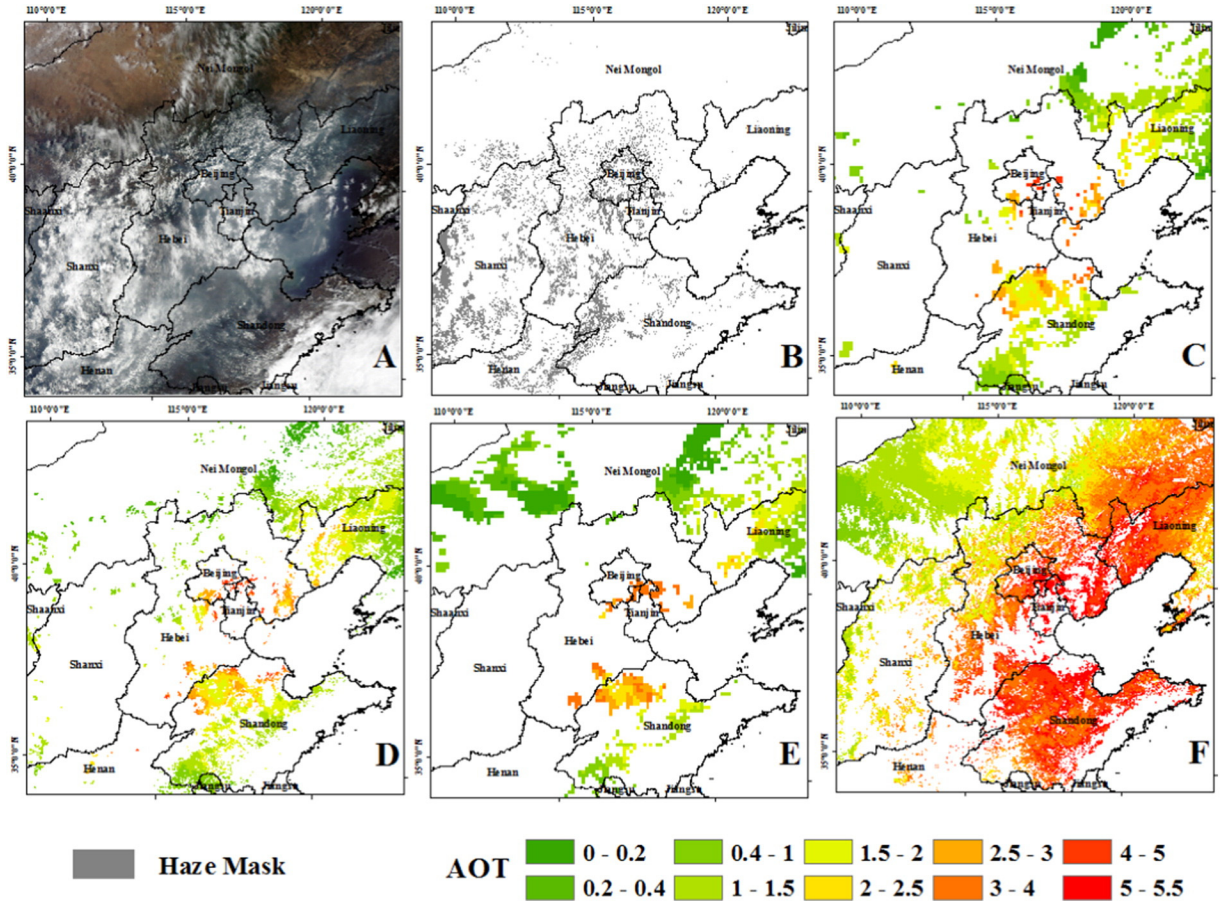

Fig. 6. (A) True-color MODIS image on 5 July 2014. (B) Result of haze identification. (C) MODIS C6 DT 10-km AOT. (D) MODIS C6 3-km AOT. (E) MODIS C6 DB 10-km AOT. (F) EHARA 1-km AOT.

densities, with low AOT values in the western region with high elevations and dense vegetation. These AOT spatial characteristics are consistent with previous research (Guo et al., 2012; Luo et al., 2015).

3.3. Validation

Fig. 8 presents the validation result of EHARA AOT, MODIS C6 DB 10-km AOT, MODIS C6 DT 10-km AOT, and MODIS C6 DT 3-km AOT with AERONET AOT. 88 AERONET measurements at 550 nm AOT (interpolated by 675 nm and 440 nm) from 2 AERONET stations Beijing and Xianghe with Level 2 data were collected over the course of ±2 to 30 min when satellite overpasses. The dotted red line is the estimated error envelope line $\pm(0.05+0.15_{\text{AERONET AOT}})$, and the solid red line is the 1:1 line. Fig. 8A compares EHARA AOT with AERONET measurements, showing the close correspondence between them. The EHARA AOT misses 3.4% of data, and the majority of the observations (73%) are within the error range $\pm(0.05+0.15_{\text{AERONET AOT}})$, which indicates that the retrieved AOT values are of good quality. Good agreement was also observed for the MODIS C6 DB AOT as most of data points lie close to the 1:1 line (Fig. 8C). It has 68% data within the error range and 9% data is missed. However, for the DT AOT products, 43% of 10-km AOT and 38% of 3-km AOT are missed in this study. In the MODIS DT 3-km AOT, only 53% of the data are within the error range line, while the 10-km AOT is 66%. Remer et al. (2013) also found that the 3-km AOT product matches AERONET less well than the 10-km product. Furthermore, Munchak et al. (2013) indicated that the performance of the 3-km AOT product is poor especially over urban surfaces, which clearly suggests a limitation for air quality applications as well.

4. Comparison and discussion

As shown in Figs. 5 and 6, the EHARA AOT had better spatial coverage than the MOD04 DT AOT products. Especially under hazy conditions, the MODIS DT aerosol products missed most values. Tao et al. (2012) found that the MODIS DT AOT could not provide a full retrieval due to haze clouds over the North China Plain, which led to an underestimation of the haze aerosol loading. Because in Section 3.2 the MODIS DB AOT also shows a good performance, thus we only focus on the comparison between the EHARA and MODIS DT AOT.

4.1. Surface reflectance assumptions

The C6 updates of the DT algorithm include refinements and code bug fixes, but they are based on the same principles as the C5 version (Sayer et al., 2014). The C6 still uses the VISvs2.1 surface reflectance parameterization with NDVIswir dependence (Levy et al., 2013), which is described in Levy et al. (2007). However, hazy days with thick aerosols make the VISvs2.1 surface reflectance relationship inappropriate (Wang et al., 2010). From Fig. 9, the NDVIswir for hazy days has a mean value of 0.381, which is significantly higher than that for non-hazy days (0.325). As presented in Eq. (8) to (10) in Levy et al. (2007), NDVIswir is the most important parameter for the calculation of surface reflectance. In hazy weather, overestimation of NDVIswir can lead to large errors in estimates of the surface reflectance of hazy pixels. Kaufman et al. (1997) indicated that an error of 0.01 in surface reflectance can lead to an error of 0.1 in retrieved AOT values. Thus, the EHARA uses MCD43 BRDF parameters to calculate surface reflectance. As shown in Fig. 1A, most elevations in the North China Plain are of less than 50 m, resulting in a low BRDF effect in the majority of urban areas. Li et al. (2013)

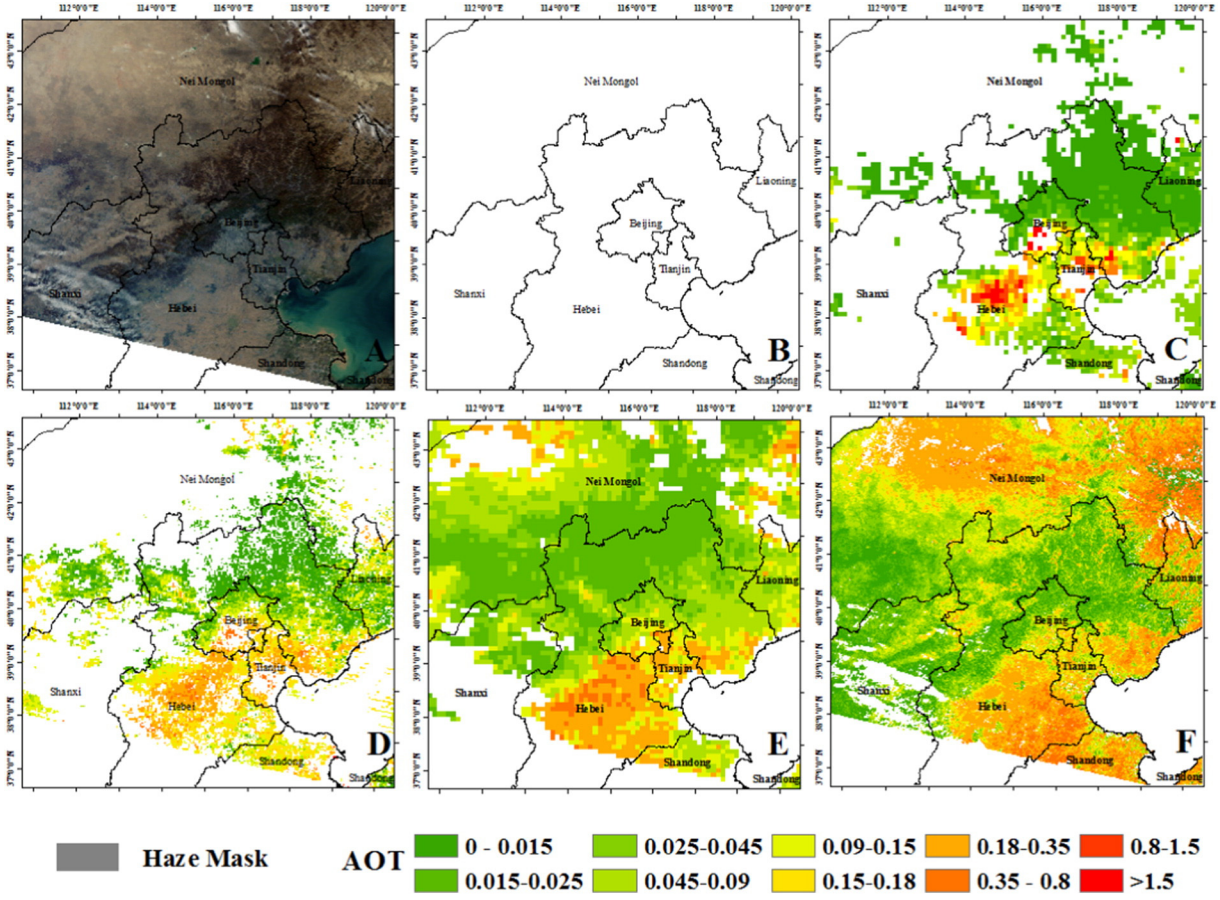

Fig. 7. (A) True-color MODIS image on 16 October 2014. (B) Results of haze identification. (C) MODIS C6 10-km AOT. (D) MODIS C6 3-km AOT. (E) MODIS C6 DB 10-km AOT. (F) EHARA 1-km AOT.

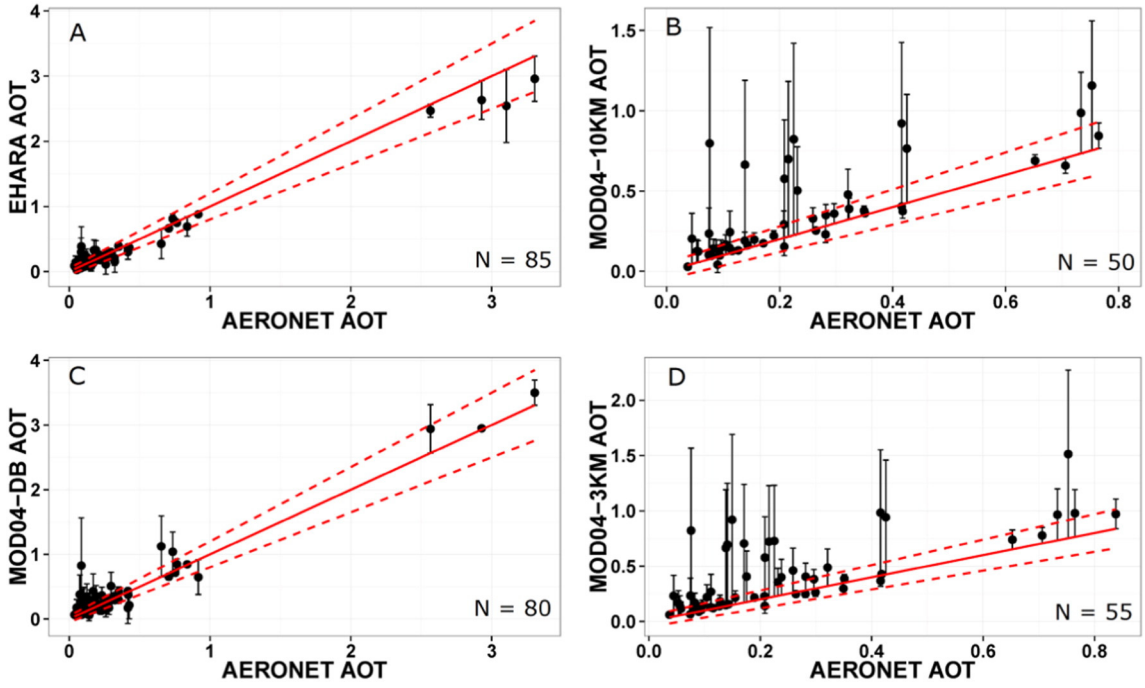

Fig. 8. Validation of AOT against AERONET (A: EHARA 1-km AOT, B: C6 DT 10-km AOT, C: C6 DB 10-km AOT, D: C6 DT 3-km AOT. Two error lines are $y = 1.15\times + 0.05$ and $y = 0.85\times - 0.05$, which correspond to the error $\Delta\tau = \pm(0.05 + 0.15_{AERONET\ AOT})$.

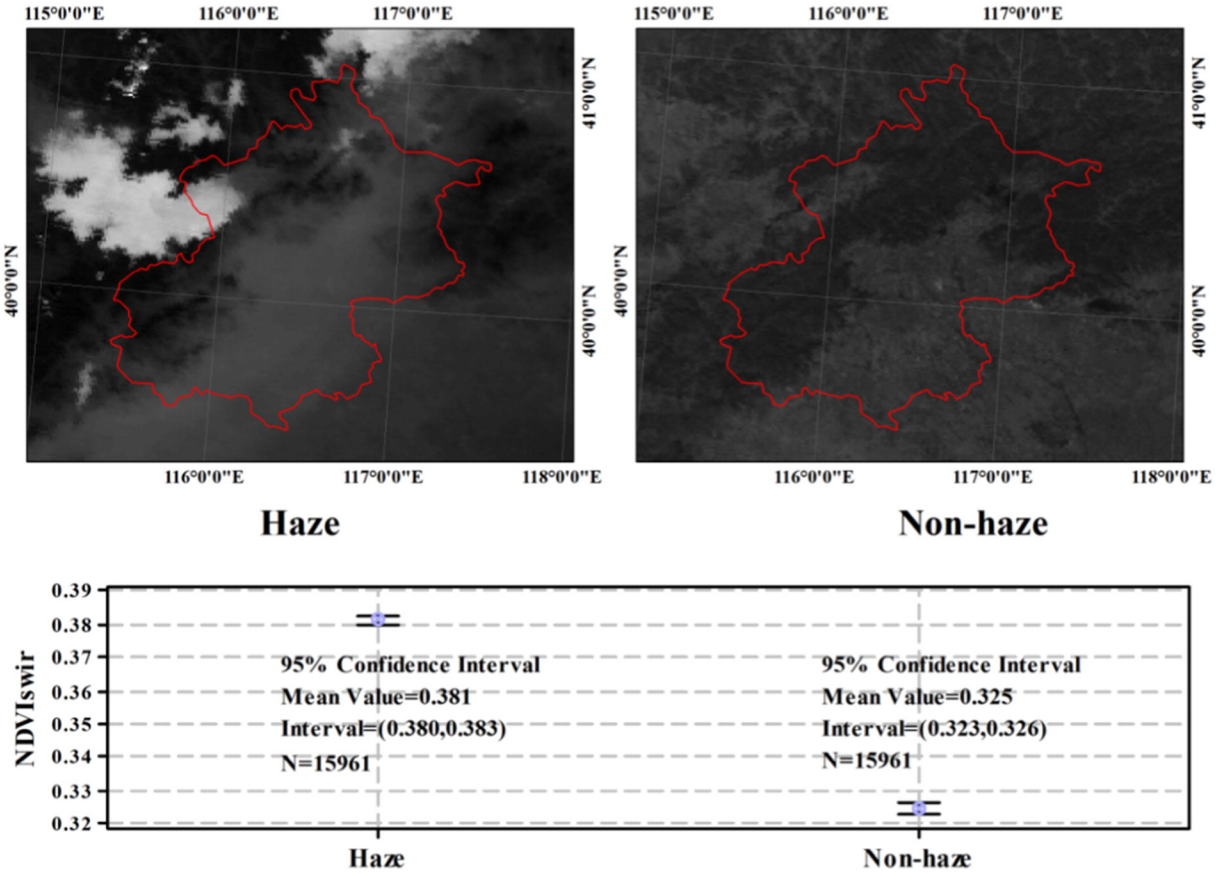

Fig. 9. NDVIswir on hazy and non-hazy days.

showed that between March and September, both mountain and urban areas have low surface reflectance and show small non-Lambertian behavior in the North China Plain; thus, errors in surface reflectance using MCD43 are likely to be less than 0.03.

4.2. Null data pixels

There are "null data" in almost every MODIS AOT image, which limit the inversion of ground-based air data like $PM_{2.5}$ and PM_{10} values. Here some brief reasons are presented for the C6 DT land algorithm to illustrate why the significant "Null Data" problem exists. A big reason for data gaps is cloud and snow cover. Second, in the C6 DT land algorithm, "dark pixels" are first selected based on 2.13-μm reflectance; fine- and coarse-mode aerosol-type LUTs are built and corrected for elevation. The LUT simulations are indexed by seven values at 550 nm AOT, which are 0.0, 0.25, 0.5, 1.0, 2.0, 3.0, and 5.0 (Levy et al., 2010). Then the inversion is conducted at 2.12-, 0.66-, and 0.47-μm wavelengths: the path and surface reflectance are a function of τ(0.55 μm), and this part of the algorithm attempts to find the surface reflectance at 2.12 μm and the value of τ at 0.55 μm. Although this should match the 0.47-μm band, the 0.66-μm band may have errors. Thus, the solution is found when the error at 0.66 μm is minimized. The exact procedure is shown as Eqs. 12–14. The calculated error evaluates the AOT retrieval result and an indicator (quality assessment, QA) is set from 0 to 3. For example, if ε is more than 0.25, QA confidence will be set at 0. As for some pixels in hazy conditions, integrated using Eqs. (12) and (14), Eq. (19) is solved and an extremely low ${\rho^*}_{0.66}$ value is obtained compared with ${\rho^m}_{0.66}$, which causes ε to exceed the limitation (0.25), and MOD04 of Optical_Depth_Land_And_Ocean only presents data of specific quality (QA confidence flag = 3).

$$\rho^{m}_{0.47}-\rho^{*}_{0.47}=0 \tag{12}$$

$$\rho^{m}_{0.66}-\rho^{*}_{0.66}=\varepsilon \tag{13}$$

$$\rho^{m}_{2.12}-\rho^{*}_{2.12}=0 \tag{14}$$

where $\rho^{*}_{0.47},\rho^{*}_{0.66},\rho^{*}_{2.12}$ are the calculated spectral total reflectance values at the top of the atmosphere, which are the weighted sums of the spectral reflectance from fine- and coarse-dominated models; $\rho^{m}_{0.47},\rho^{m}_{0.66},\rho^{m}_{2.12}$ are the MODIS measured reflectance values.

Third, the C6 DT algorithm includes a thin-cirrus test to determine clouds which may lead to aerosol contamination. Pixels with $\rho_{1.38}>0.01$are deemed to be "thin cirrus" and the QA confidence of these pixels is then reduced to zero. The C6 also updates the code such that AOT values close to a cloudy area are not retrieved. For example, as shown in Fig. 6A and B, hazy weather is usually accompanied by clouds; thus, C6 may miss haze aerosol retrieval in areas of "thin cirrus" or close to clouds.

Several "null data" AOT pixels may be acquired using the EHARA method, as shown in Fig. 10B. The reason is that aerosol and Rayleigh reflectance ($\rho_{Aer}(\theta_0,\theta,\phi),\rho_{Ray}(\theta_0,\theta,\phi)$) are obtained by experience formulas (Eqs. 6 and 8), which may lead to $\rho_{TOA(\lambda)}(\theta_0,\theta,\phi)-\rho_{Aer}(\theta_0,\theta,\phi)-\rho_{Ray}(\theta_0,\theta,\phi)<0$ in some pixels. This may be related to the influence of weather and viewing angle. Nevertheless, this phenomenon is significantly less evident than in MODIS DT aerosol products, as shown in Fig. 10B and D.

4.3. Differences in aerosol models

The C6 aerosol products have been updated with new aerosol type selections; however, their overall spatial distribution remains the same as defined for the C5 version (Levy et al., 2013). The weakly

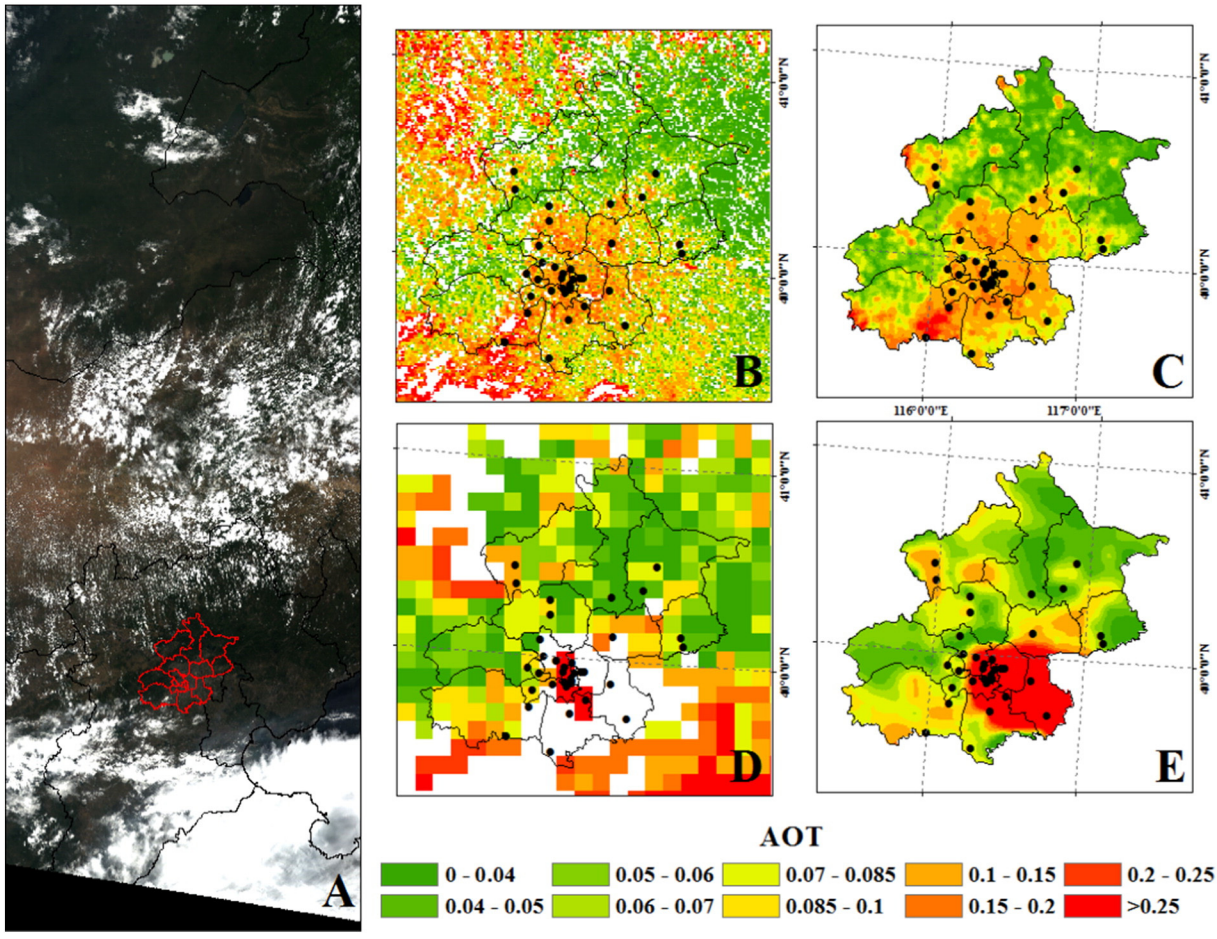

Fig. 10. (A) True-color MODIS image on 12 July 2014. (B) EHARA AOT values. (C) Interpolation of EHARA AOT and (D) MODIS C6 DT 10-km AOT values. (E) Interpolation of MODIS C6 DT 10-km AOT values (black dots are Beijing environmental monitoring stations.)

absorbing (SSA = 0.95) and the moderately absorbing (SSA = 0.91) aerosol models in C6 are generally adopted for the North China Plain (Levy et al., 2010). However, the EHARA uses intraday AERONET SSA to retrieve AOT. Another issue for the MODIS DT land retrieval algorithm is that it often selects the dust aerosol model over land areas where dust is unlikely to be found. This is especially likely when AOT values are small (Mielonen et al., 2011).

4.4. Application to air quality assessment

To assess air pollution levels at large scales, the relationship between satellite-based AOT values and ground-based air-pollution data, including air quality index (AQI) $PM_{2.5}$ and PM_{10} values, is useful. However, as shown in Fig. 10D, the C6 aerosol products omit a number of the Beijing environmental monitoring stations, which obstructs the spatial assessment of air pollution and the mapping of air quality. To solve this problem, interpolation is conducted, as shown in Fig. 10E. Nevertheless, it is clear that the resulting AOT spatial distribution differs from that in Fig. 10C. The inappropriate interpolation is due to the large number of missing values southeast of Beijing. Additionally, the contrast between Fig. 10B and D indicates that EHARA AOT values are more spatially complete than the C6 AOT values. Fig. 10B and C shows that using interpolation for the null EHARA AOT data results in almost the same spatial distribution as the original data. Moreover, most importantly, the EHARA can provide better performance for AOT values on hazy days and result in more appropriate air quality assessment. Another problem for the C6 AOT application is that of output of negative values. It should be noted that the MODIS retrieval algorithm permits negative AOT values, and negative retrieval results are especially common on days with low-AOT values (Hyer et al., 2011).

5. Conclusions

This study developed the EHARA to retrieve AOT values and compare them with the latest MODIS C6 aerosol products. Based on 12 years of AERONET data, we proposed empirical SSA and AF values for haze aerosol retrieval: 0.9 (SSA) and 0.71 (AF) for the blue band, and 0.92 (SSA) and 0.67 (AF) for the red band. Comparison with ground-based AERONET data showed that EHARA-derived AOT had a fine spatial resolution of 1-km and a high level of accuracy (73% within error range and 3.4% missed value), which is higher than MODIS C6 DT 10-km (66% within error range and 43% missed value) and 3-km (53% within error range and 38% missed value) aerosol products. In this study, the C6 DB also has a good performance under haze or normal weather days (68% within error range and 9% missed value). The main reasons for the high accuracy of the EHARA are thought to be the use of real time AERONET data to determine the aerosol model (SSA and AF values) and the differences in assumptions regarding surface reflectance. Additionally, because of its haze detection, the EHARA can assign an appropriate aerosol model for haze pixels, and successfully retrieve more AOT values on hazy days. This paper also discussed the differences between the EHARA and MODIS C6 DT land algorithm in detail. The main limitations for the MODIS C6 DT aerosol products are related to "null data" and negative AOT values. This study offers a fast and effective method for investigating aerosol spatial distributions at large scales, especially for haze aerosol monitoring. Environmental authorities can

use this method for aerosol distribution mapping and air quality assessment in large areas.

Acknowledgments

This work was supported in part by the National Natural Science Foundation of China under Grant 41201451 and Grant 40901214, in part by the Ministry of Science and Technology of China (Project no: 2012BAJ15B04 and 2012AA12A305). The authors would like to acknowledge the MODIS and AERONET Teams for their effort in making the data available. The authors are grateful to Dr. Andrew Sayer for important suggestions and comments related to this paper.

References

Antoine, D., Morel, A., 1998. Relative importance of multiple scattering by air molecules and aerosols in forming the atmospheric path radiance in the visible and near-infrared parts of the spectrum. Appl. Opt. 37, 2245–2259.

Bergin, M.H., Cass, G.R., Xu, J., Fang, C., Zeng, L.M., Yu, T., Salmon, L.G., Kiang, C.S., Tang, X.Y., Zhang, Y.H., Chameides, W.L., 2001. Aerosol radiative, physical, and chemical properties in Beijing during June 1999. J. Geophys. Res. Atmos. 106, 17696–17980.

Che, H.Z., Zhang, X.Y., Li, Y., Zhou, Z.J., Qu, J.J., Hao, X.J., 2009. Haze trends over the capital cities of 31 provinces in China, 1981–2005. Theor.Appl.Climatol. 97, 235–242.

Drury, E., Jacob, D.J., Wang, J., Spurr, R.J.D., Chance, K., 2008. Improved algorithm for MODIS satellite retrievals of aerosol optical depths over western North America. J. Geophys. Res. 113, D16204.

Guo, Y., Hong, S., Feng, N., Zhuang, Y., Zhang, L., 2012. Spatial distributions and temporal variations of atmospheric aerosols and the affecting factors: a case study for a region in central China. Int. J. Remote Sens. 33, 3672–3692.

Han, L., Tsunekawa, A., Tsubo, M., Zhou, W., 2013. An enhanced dust index for Asian dust detection with MODIS images. Int. J. Remote Sens. 34, 6484–6495.

Hoek, G., et al., 2010. Concentration response functions for ultrafine particles and all-cause mortality and hospital admissions: results of a European expert panel elicitation. Environ. Sci. Technol. 44 (1), 476–482.

Hsu, N.C., Jeong, M.-J., Bettenhausen, C., Sayer, A.M., Hansell, R., Seftor, C.S., Huang, J., Tsay, S.-C., 2013. Enhanced deep blue aerosol retrieval algorithm: the second generation. J. Geophys. Res.-Atmos. 118, 9295–9315.

Huang, K., Zhuang, G., Lin, Y., Fu, J.S., Wang, Q., Zhang, R., Jiang, Y., Deng, C., Fu, Q., Hsu, N.C., Cao, B., 2012. Typical types and formation mechanisms of haze in eastern Asia megacity, Shanghai. Atmos. Chem. Phys. 12, 105–124.

Huang, K.L., Yuan, C.S., Wang, G.Z., Wang, K., 2011. Chemical characteristics and source apportionment of PM(10) during a brown haze episode in Harbin, China. Particuology 9, 32–38.

Hyer, E.J., Reid, J.S., Zhang, J., 2011. An over-land aerosol optical depth data set for data assimilation by filtering, correction, and aggregation of MODIS Collection 5 optical depth retrievals. Atmos. Meas. Tech. 4, 379–408.

Kaufman, Y.J., Tanré, D., Gordon, H.R., Nakajima, T., Lenoble, J., Frouin, R., Grassl, H., Herman, B.M., King, M.D., Teillet, P.M., 1997. Passive remote sensing of tropospheric aerosol and atmospheric correction for the aerosol effect. J. Geophys. Res.-Atmos. 102 (D14), 16815–16830.

Lee, H.K., Kim, Y.J., Kim, M.J., 2006a. Characteristics of aerosol observed during two severe haze events over Korea in June and October 2004. Atmos. Environ. 40, 5146–5155.

Lee, K.H., Kim, Y.J., Kim, J., von Hoyningen-Huene, W., Burrow, J.P., 2006b. Influence of land surface effects on MODIS aerosol retrieval using the BAER method over Korea. Int. J. Remote Sens. 27, 2813–2830.

Levy, R.C., Mattoo, S., Munchak, R.L.A., Sayer, A.M., Patadia, F., Hsu, N.C., 2013. The Collection 6 MODIS aerosol products over land and ocean. Atmos. Meas. Tech. 6, 2989–3034.

Levy, R.C., Remer, L.A., Kleidman, R.G., Mattoo, S., Ichoku, C., Kahn, R., Eck, T.F., 2010. Global evaluation of the Collection 5 MODIS dark-target aerosol products over land. Atmos. Chem. Phys. 10, 10399–10420.

Levy, R.C., Remer, L.A., Mattoo, S., Vermote, E.F., Kaufman, Y.J., 2007. Second-generation operational algorithm: retrieval of aerosol properties over land from inversion of moderate resolution imaging spectroradiometer spectral reflectance. J. Geophys. Res.-Atmos. 112, D13211.

Li, C.C., Lau, A.K., Mao, J.T., et al., 2005. Retrieval, validation and application of the 1-km aerosol optical depth from MODIS measurement over Hong Kong. IEEE Trans. Geosci. Remote Sens. 43, 2650–2658.

Li, S.S., Chen, L.F., Xiong, X.Z., Tao, J.H., Su, L., Han, D., Liu, Y., 2013. Retrieval of the haze optical thickness in north China plain using MODIS data. IEEE Trans. Geosci. Remote Sens. 51, 2528–2540.

Liu, C.H., Liu, G.R., 2009. Aerosol optical depth retrieval for SPOT HRV images. J. Mar. Sci. Technol. 17, 300–305.

Luo, N.N., Wong, M.S., Zhao, W.J., Yan, X., Xiao, F., 2015. Improved aerosol retrieval algorithm using Landsat images and its application for PM10 monitoring over urban areas. Atmos. Res. 153, 264–275.

Mao, J., Li, C., 2005. Observation study of aerosol radiative properties over China. Acta Metall. Sin. 63, 622–635.

Mielonen, T., Levy, R.C., Aaltonen, V., Komppula, M., Gde, L., Huttunen, J., Lihavainen, H., Kolmonen, P., Lehtinen, K.E.J., Arola, A., 2011. Evaluating the assumptions of surface reflectance and aerosol type selention within the MODIS aerosol retrieval over land: the problem of dust type selection. Atmos. Meas. Tech. 4, 201–214.

Munchak, L.A., Levy, R.C., Mattoo, S., Remer, L.A., Holben, B.N., Schafer, J.S., Hostetler, C.A., Ferrare, R.A., 2013. MODIS 3 km aerosol product: applications over land in an urban/suburban region. Atmos. Meas. Tech. 6, 1747–1759.

Noh, Y.M., Muller, D., Shin, D.H., Lee, H., Jung, J.S., Lee, H.K., Cribb, M., Li, Z.Q., Kim, Y.J., 2009. Optical and microphysical properties of severe haze and smoke aerosol measured by integrated remote sensing techniques in gwangju, Korea. Atmos. Environ. 43, 879–888.

Rahman, H., Pinty, B., Verstraete, M.M., 1993. Coupled surface-atmosphere reflectance (CSAR) model: 2. Semiempirical surface model usable with NOAA advanced very high resolution radiometer data. J. Geophys. Res.-Atmos. 98, 20791–20801.

Ram, S.S., Kumar, R.V., Chaudhuri, P., Chanda, S., Santra, S.C., Sudarshan, M., Chakraborty, A., 2014. Physico-chemical characterization of street dust and re-suspended dust on plant canopies: an approach for finger printing the urban environment. EcolIndic 36, 334–338.

Remer, L.A., Mattoo, S., Levy, R.C., Munchak, L.A., 2013. MODIS 3 km aerosol product: algorithm and global perspective. Atmos. Meas. Tech. 6, 1829–1844.

Roujean, J.L., Leroy, M., Deschamps, P.Y., 1992. A bi-directional reflectance model of the earth's surface for correction of remote sensing data. J. Geophys. Res.-Atmos. D97, 20455–20468.

Sayer, A.M., Hsu, N.C., Bettenhausen, C., M-j, J., 2013. Validation and uncertainty estimates for MODIS collection 6 “deep blue” aerosol data. J. Geophys. Res.-Atmos. 118, 7864–7873.

Sayer, A.M., Munchak, L.A., Hsu, N.C., Levy, R.C., Bettenhausen, C., Jeong, M.J., 2014. MODIS Collection 6 aerosol products: comparison between aqua's e-deep blue, dark target, and “merged” data sets, and usage recommendations. J. Geophys. Res.-Atmos. 119, 13965–13989.

Sun, Y., Zhuang, G., Tang, A., Wang, Y., An, Z., 2006. Chemical characteristics of PM2.5 and PM10 in haze-fog episodes in Beijing. Environ. Sci. Technol. 4, 1383–1395.

Tang, J.K., Xue, Y., Yu, T., Guan, Y.N., 2005. Aerosol optical thickness determination by exploiting the synergy of terra and aqua MODIS (SYNTAM). Remote Sens. Environ. 94, 327–334.

Tanre, D., Herman, M., Deschamps, P.Y., Leffe, A., 1979. Atmospheric modeling for space measurements of ground reflectances, including bidirectional properties. Appl. Opt. 18, 3587–3594.

Tao, M.H., Chen, L.F., Su, L., Tao, J.H., 2012. Satellite observation of regional haze pollution over the North China Plain. J. Geophys. Res.-Atmos. 117, D12203.

Tao, M.H., Chen, L.F., Wang, Z.F., Tao, J.H., Su, L., 2013. Satellite observation of abnormal yellow haze clouds over East China during summer agricultural burning season. Atmos. Environ. 79, 632–640.

Tao, M.H., Chen, L.F., Xiong, X.Z., Ma, P.F., Tao, J.H., Wang, Z.F., 2014. Formation process of the widespread extreme haze pollution over northern China in January 2013: implications for regional air quality and climate. Atmos. Environ. 98, 417–425.

Wang, J., Xu, X.G., Spurr, R., Wang, Y., Drury, E., 2010. Improved algorithm for MODIS imagery over land surface. Remote Sens. Environ. 114, 2575–2583.

Wong, M.S., Nichol, J.E., Lee, K.H., 2011. An operational MODIS aerosol retrieval algorithm at high spatial resolution, and its application over a complex urban region. Atmos. Res. 99, 579–589.

Yan, P., Tang, J., Huang, J., et al., 2008. The measurement of aerosol optical properties at a rural site in Northern China. Atmos. Chem. Phys. 8, 2229–2242.

Yu, X., Li, X., Deng, Z., De, Q., Shuai, Y., 2012. Optical properties of aerosol during haze-fog episodes in Beijing. Environ. Sci. 33, 1057–1062.

Zha, Y., Wang, Q., Yuan, J., Gao, Y., Jiang, J.J., Lu, H., Huang, J., 2011. Improved retrieval of aerosol optical thickness from MODIS measurements through derived surface reflectance over Nanjing, China. Tellus 58B, 952–958.